High-codimensional knots spun about manifolds

DENNIS ROSEMAN
MASAMICHI TAKASE

Using spinning we analyze in a geometric way Haefliger's smoothly knotted $(4k-1)$–spheres in the $6k$–sphere. Consider the 2–torus standardly embedded in the 3–sphere, which is further standardly embedded in the 6–sphere. At each point of the 2–torus we have the normal disk pair: a 4–dimensional disk and a 1–dimensional proper subdisk. We consider an isotopy (deformation) of the normal 1–disk inside the normal 4–disk, by using a map from the 2–torus to the space of long knots in 4–space, first considered by Budney. We use this isotopy in a construction called *spinning about a submanifold* introduced by the first-named author. Our main observation is that the resultant spun knot provides a generator of the Haefliger knot group of knotted 3–spheres in the 6–sphere. Our argument uses an explicit construction of a Seifert surface for the spun knot and works also for higher-dimensional Haefliger knots.

57R40; 57R65, 55P35

1 Introduction

Various kinds of spinning constructions, all of which stem from Artin's original construction [1], are now basic tools in the study of high-dimensional knots in *codimension two*, that is, in the study of embeddings of n–manifolds in the $(n+2)$–sphere.

On another front, Haefliger [11; 12] found smooth knots in *codimensions greater than two*. He showed that the group C^q_n of isotopy classes of smooth embeddings of the n–sphere S^n into $(n+q)$–sphere S^{n+q} is often non-trivial even when $q \geq 3$. Although many spinning constructions can be applied for such "high-codimensional" knots, there have been very few related studies (see Budney [4], Hsiang and Sanderson [13] and Milgram [15]).

Budney [4] gave a new description of a generator of the Haefliger knot group C^3_3. This was related to his study on the space $\mathcal{K}_{4,1}$ of "long" knots in 4–space. Here, $\mathcal{K}_{n,j}$ is the space of *long knots* — smooth embeddings of $\mathbb{R}^j \hookrightarrow \mathbb{R}^n$ which are standard outside the unit disk in $\mathbb{R}^j$. We note that the restriction of a long embedding to the unit disk gives a properly embedded j–disk in the unit n–disk — our construction will refer to it. In his paper, a map (the resolution map) $\Phi\colon T^2 \to \mathcal{K}_{4,1}$ from the

Published: 25 April 2007 DOI: 10.2140/agt.2007.7.359

2–torus T^2, defined in an ingenious way (see Section 2.2), plays a key role. This map gives rise to generators of certain homotopy groups and of the Haefliger group, via successive graphing constructions. The geometric nature of graphing constructions here is a high-codimensional version of Litherland's deform-spinning [14].

We give yet another description of a generator of the Haefliger knot group C^3_3 in terms of the notion *spinning about a submanifold*, introduced by the first-named author [16]. Our main result is as follows (see Section 3 for the details). Consider the 2–torus T^2 standardly embedded in S^3, which is further standardly embedded in S^6. At each point of T^2, we have the normal 4–disk D^4 to $T^2 \subseteq S^6$ and the normal 1–disk D^1 to $T^2 \subseteq S^3$. Then, we "deform" D^1 inside D^4, by using Φ. Namely, at each point of $\tau \in T^2$, we replace the standard disk pair (D^4, D^1) with the new disk pair $(D^4, \Phi(\tau)(D^1))$. We then show that the resultant smoothly embedded 3–sphere $\Sigma^3_\Phi \subseteq S^6$ represents a generator of the Haefliger knot group C^3_3.

Our study is motivated by Budney's construction and in particular his resolution map $\Phi\colon T^2 \to \mathcal{K}_{4,1}$. Our approach is different. We use a basic technique in the spirit of codimension two knot theory — examination of how the homology of a Seifert surface relates to the knot complement. It is very geometric, uses higher-dimensional visualization, does not involve any homotopy groups and might be useful for more general high-codimensional knots.

Additionally, all of Budney's and our arguments work for higher-dimensional Haefliger knot groups C^{2k+1}_{4k-1}, $k \geq 2$. We need just to consider the triple

$$S^{2k-1} \times S^{2k-1} \subseteq S^{4k-1} \subseteq S^{6k}$$

and use everywhere a higher-dimensional Budney map [4, Section 3]

$$S^{2k-1} \times S^{2k-1} \to \mathcal{K}_{2k+2,1}$$

instead of $\Phi\colon T^2 = S^1 \times S^1 \to \mathcal{K}_{4,1}$.

Throughout the paper, we work in the smooth category; all manifolds and mappings are supposed to be differentiable of class C^∞, unless otherwise stated. We use the symbol '$\cong$' for a group isomorphism and '$\approx$' for a diffeomorphism.

The authors would like to thank the referee for his or her careful reading and suggestions which greatly improved the exposition of this paper. The second-named author would like to thank Ryan Budney for fruitful conversations. The second-named author is partially supported by the Iwanami Fujukai Foundation and by the Sumitomo Foundation.

2 Preliminaries

2.1 Haefliger's knots

Haefliger showed in [11; 12] that the group C^n_q of smooth isotopy classes of smooth embeddings of the n–sphere S^n in the $(n+q)$–sphere S^{n+q} is often non-trivial even when the codimension q is greater than 2. In a particular case, for each $k \geq 1$ the group C^{4k-1}_{2k+1} of smooth isotopy classes of smooth embeddings $S^{4k-1} \hookrightarrow S^{6k}$ forms the infinite cyclic group $\mathbb{Z}$. This is in contrast with Zeeman's unknotting theorem [20] stating that any n–sphere is unknotted in the *piecewise linear* sense in the $(n+q)$–sphere if $q > 2$.

According to Boéchat and Haefliger [2; 3] and the second-named author [19; 18], the smooth isotopy class of Haefliger's knot can be read off from geometric characteristics of its Seifert surface. When $k = 1$, we have the following (see Guillou–Marin [10] and Boéchat–Haefliger [3]).

Theorem 2.1 *Every embedding $F\colon S^3 \hookrightarrow S^6$ has a Seifert surface $\widetilde{F}\colon V^4 \hookrightarrow S^6$ and*

$$\mathsf{H}(F) = -\tfrac{1}{8}\big(\sigma(V^4) - e_{\widetilde{F}} \smile e_{\widetilde{F}}\big)$$

gives the isomorphism $\mathsf{H}\colon C^3_3 \to \mathbb{Z}$, where $e_{\widetilde{F}}$ denotes the normal Euler class of $\widetilde{F}$.

2.2 Budney's isomorphism

Several papers, including those by Boéchat [2], Boéchat–Haefliger [3], Guillou–Marin [10], the second author [19; 18], and Skopenkov [17], give geometric descriptions for the Haefliger knot groups C^{2k+1}_{4k-1} and their generators. Recently, Budney [4] has given a description of such Haefliger knots in terms of the space of long knots, which is related to the Litherland-type deform-spinning.

Let $\mathcal{K}_{n,j}$ be the space of smooth embeddings (*long embeddings*) $\mathbb{R}^j \hookrightarrow \mathbb{R}^n$ being the standard inclusions on $|x| \geq 1$ for $x \in \mathbb{R}^j$. Then, Budney [4], using results of Goodwillie [9], showed that there is an isomorphism $\pi_2\mathcal{K}_{4,1} \to C^3_3$. His isomorphism gives a new description of the Haefliger group $C^3_3 \approx \mathbb{Z}$.

We briefly review Budney's construction. Note that he deals with more general cases in [4, Section 3], so that he constructs an epimorphism $\pi_{2d-2}\mathcal{K}_{d+2,1} \to C^{d+1}_{2d-1}$ (for $d > 1$), which gives an isomorphism when d is even.

2.2.1 The graphing map Consider the "graphing" map $\mathrm{gr}_1\colon \Omega\mathcal{K}_{n-1,j-1} \to \mathcal{K}_{n,j}$ defined by

$$(\mathrm{gr}_1 f)(t_0, t_1, \ldots, t_{j-1}) = (t_0, f(t_0)(t_1, \ldots, t_{j-1})).$$

Budney [4] showed that the maps $\Omega\mathcal{K}_{4,1} \to \mathcal{K}_{5,2}$ and $\Omega\mathcal{K}_{5,2} \to \mathcal{K}_{6,3}$ induce isomorphisms

$$\pi_2\mathcal{K}_{4,1} \cong \pi_1\mathcal{K}_{5,2} \cong \pi_0\mathcal{K}_{6,3}.$$

Furthermore, the group $\pi_0\mathcal{K}_{6,3}$ is isomorphic to C_3^3 due to Haefliger [12].

2.2.2 The resolution map $\Phi\colon T^2 \to \mathcal{K}_{4,1}$ Take a "long" immersion $f\colon \mathbb{R} \to \mathbb{R}^3 \subseteq \mathbb{R}^4$ such that $f(t) = (t, 0, 0, 0)$ for $|t| > 1$ and has two double points $f(t_1) = f(t_3)$, $f(t_2) = f(t_4)$ with $-1 < t_1 < t_2 < t_3 < t_4 < 1$ and such that $df(T_{t_1}\mathbb{R}) \cap df(T_{t_3}\mathbb{R}) = df(T_{t_2}\mathbb{R}) \cap df(T_{t_4}\mathbb{R}) = \{0\}$ (see Figure 1). At $f(t_1) = f(t_3)$ and $f(t_2) = f(t_4)$, we have the 2–dimensional normal complements P_1 to $df(T_{t_1}\mathbb{R}) \oplus df(T_{t_3}\mathbb{R})$ and P_2 to $df(T_{t_2}\mathbb{R}) \oplus df(T_{t_4}\mathbb{R})$, respectively.

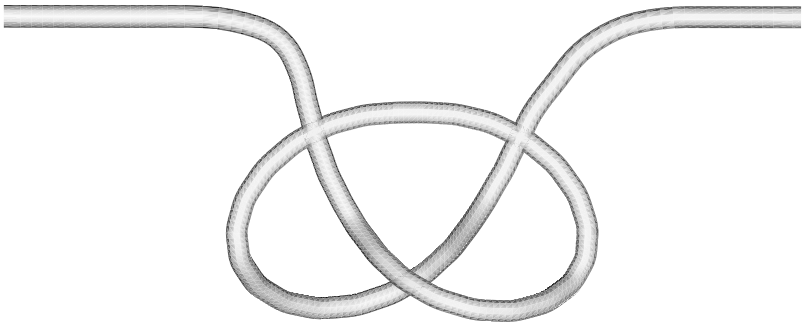

Figure 1: An immersed long line with two intersections, thickened and shown as a thin tube.

Let S_1 and S_2 be the unit 1–dimensional sphere in P_1 and P_2 respectively. Given $(\theta, \psi) \in S_1 \times S_2$, we perturb a small neighborhood of $f(t_1)$ in direction θ using a bump function and a small neighborhood of $f(t_2)$ with ψ. In this way, we can eliminate the double points, separating via a fourth dimension. Thus we obtain a "resolution map"

$$\Phi\colon T^2 = S_1 \times S_2 \to \mathcal{K}_{4,1}.$$

Finally, Budney, Conant, Scannell and Sinha [5] showed that Φ generates $H_2(\mathcal{K}_{4,1}; \mathbb{Z})$ and hence generates $\pi_2\mathcal{K}_{4,1} \cong \mathbb{Z}$ since $\mathcal{K}_{4,1}$ is simply-connected.

2.3 Deform-spinning about a submanifold

The spinning describes several methods of constructing higher-dimensional knots from lower-dimensional knots. The most fundamental method, simply called *spinning*, is due to Artin [1]. It has been generalized in various ways (a useful reference in this area is Friedman [8]). In this paper, we will use the *deform-spinning about a submanifold* (in [8] called *frame deform-spinning*), introduced by the first-named author [16].

Definition 2.2 Suppose M^k is a submanifold of $S^p \subseteq S^q$ with trivial tubular neighborhood $N \approx M^k \times D^{p-k} \subseteq S^p$. Then M has a trivial tubular neighborhood $T \approx M^k \times D^{q-k}$ in S^q. We can write:

$$(T, N) = M^k \times (D^{q-k}, D^{p-k}).$$

Suppose $\Phi\colon M^k \to \mathcal{K}_{q-k,p-k}$ is a smooth map. The *deform spun knot* Σ_Φ *about* M^k is the embedded p–sphere in S^q, obtained from $S^p \subseteq S^q$ by replacing the standard ball pair $\{x\}\times(D^{q-k}, D^{p-k})$ with $\{x\}\times(D^{q-k}, \Phi(x)(D^{p-k}))$ at each point $x \in M^k$.

This generalizes Litherland's *deform-spinning* [14], that corresponds to the case where M^k is taken as S^1 standardly embedded in $S^p \subseteq S^{p+2}$.

Deform-spinning about a submanifold is one of the most generalized forms of spinning. For example, we can describe Artin's original spinning as Σ_Φ where $M^k = S^1$ in $S^2 \subseteq S^3$ and Φ is a constant map. A *super-spun* p–knot (see Cappell [6]) is given by deform-spinning about $M^k = S^k \subseteq S^p$ with a constant map Φ. Zeeman's *twist-spun* knot [21] is a deform-spun knot about $M^k = S^1 \subseteq S^2 \subseteq S^3$ via the map $\Phi\colon S^1 \to \mathcal{K}_{3,1}$; where $\Phi(\theta)$ is the rotated image of a knotted arc about the x–axis by an angle of θ. Another variation is Fox's *roll-spinning* [7]. Yet another extension *spinning of a knot about a projection of a knot* uses a mapping of a manifold into S^p [16].

3 The main theorem

Consider the 2–torus $\mathbb{T}^2$ standardly embedded in S^3, which is further included in S^6 in the standard manner: $\mathbb{T}^2 \subseteq S^3 \subseteq S^6$. At each point of $\mathbb{T}^2$ we consider the normal 4–disk to $\mathbb{T}^2 \subseteq S^6$ and the normal 1–disk to $\mathbb{T}^2 \subseteq S^3$, which form the standard disk pair (D^4, D^1).

We can deform-spin $S^3 \subseteq S^6$ about the torus $\mathbb{T}^2 \subseteq S^3 \subseteq S^6$ with Budney's resolution map (Section 2.2.2) $\Phi\colon \mathbb{T}^2 \to \mathcal{K}_{4,1}$. In the normal plane at each point $\tau \in \mathbb{T}^2$, we

replace the standard disk pair (D^4, D^1) with a new disk pair $(D^4, \Phi(\tau)(D^1))$. We denote the resultant embedded 3–sphere in S^6 by Σ^3_Φ. Namely, in S^6

$$\Sigma^3_\Phi \quad = \quad \overline{S^3 \smallsetminus (\mathbb{T}^2 \times D^1)} \cup \bigcup_{\tau \in \mathbb{T}^2} \Phi(\tau)(D^1).$$

Let $J\colon S^3 \hookrightarrow S^6$ be a smooth embedding so that $J(S^3) = \Sigma^3_\Phi \subseteq S^6$. Then, our main theorem is the following:

Theorem 3.1 $\mathsf{H}(J) = \pm 1$; *J represents a generator of $C^3_3 \cong \mathbb{Z}$.*

4 A Seifert surface and the proof

Consider the 2–torus $\mathbb{T}^2 \subseteq S^3 \subseteq S^6$, along which we performed the spinning, to be

$$\mathbb{T}^2 = S^1_\theta \times S^1_\psi = \{(\theta, \psi); \theta, \psi \in \mathbb{R}/2\pi\mathbb{Z}\}.$$

At each point $(\theta, \psi) \in \mathbb{T}^2$, we identify the normal 4–disk $D^4_{(\theta,\psi)}$ to $\mathbb{T}^2 \subseteq S^6$ with the unit disk D^4 in $\mathbb{R}^4 = \{(x, y, z, w)\}$. Thus, $((\theta, \psi), (x, y, z, w))$ gives a coordinate system for a tubular neighborhood (diffeomorphic to $\mathbb{T}^2 \times D^4$) of $\mathbb{T}^2$ in S^6.

Let $\mathbb{B}^4$ be the northern hemisphere of $S^4 \subseteq S^6$, which we think of as the standard Seifert surface for the unknot $S^3 \subseteq S^6$. We can assume that in each normal 4–disk $D^4_{(\theta,\psi)}$ to $\mathbb{T}^2 \subseteq S^6$, the 4–disk $\mathbb{B}^4$ is seen as in Figure 2, which depicts the hyperplane section by $w = 0$ of $D^4_{(\theta,\psi)}$ and where the intersection of $\mathbb{B}^4$ and $D^4_{(\theta,\psi)}$ is shown in gray. We denote this intersection $\mathbb{B}^4 \cap D^4_{(\theta,\psi)}$ by $\mathbb{B}^2_{\theta,\psi}$.

4.1 A Seifert surface

To construct a Seifert surface for our spun knot $\Sigma^3_\Phi \subseteq S^6$, we first consider the punctured 2–dimensional torus in the 4–disk $D^4_{(0,0)}$, as shown in Figure 3. In Figure 3, Σ^3_Φ is the arc drawn with a thick line. We remark that although this arc appears knotted since it is pictured in three-dimensional space, it is really smoothly unknotted in $D^4_{(0,0)}$. We view $\mathring{T}_{(0,0)}$ in a standard way as a 2–disk C with two bands A and B, as in Figure 4. The figures show piecewise smooth objects which, by standard methods in differential topology, correspond to unique smooth objects.

In the normal 4–disk $D^4_{(\theta,\psi)}$ for general $(\theta, \psi) \in \mathbb{T}^2$, we consider the embedded punctured 2–torus $\mathring{T}_{(\theta,\psi)}$, defined as follows. The punctured torus $\mathring{T}_{(\theta,\psi)}$ coincides with $\mathring{T}_{(0,0)}$ on the disk C and differs from $\mathring{T}_{(0,0)}$ only on the two bands A and B. In the punctured torus $\mathring{T}_{(\theta,\psi)}$, the band A has been replaced with A_θ and B has been

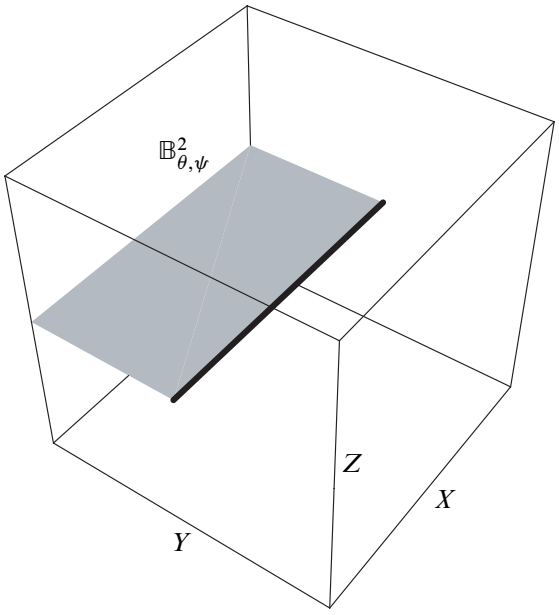

Figure 2: For any values of (θ, ψ), the standard Seifert surface of the unknot is as shown. The center point of the cube has coordinates $(0, 0, 0, 0)$; the last coordinate w is not shown.

replaced with B_ψ: $\mathring{T}_{(\theta,\psi)} = C \cup A_\theta \cup B_\psi$. Now we describe the band A_θ in detail; B_ψ will be treated similarly.

We obtain A_θ by rotating A around the 2–dimensional axis $\{w = z = 0\}$ by an angle of $\gamma(y)\theta$, where $\gamma(y)$ is a smooth bump function with $\gamma(y) = 0$ in a neighborhood of ± 1 and $\gamma(y) = 1$ for $-1/4 \le y \le 1/4$ (see Figure 5). So γ allows us to smoothly attach the band A_θ to C. If we only consider the motion of the edges of the band A in the above process, it corresponds to Budney's resolution process (see Section 2.2.2) for one intersection point.

To clarify this construction, we show $\mathring{T}_{(\pi,0)}$ in Figure 6. In the generic case, the rotation will move points not in the center of the band so that it has non-zero w–coordinate and the points of $\mathring{T}_{(\theta,\psi)}$ in $\{w = 0\}$ is shown in Figure 7.

Putting together all the punctured tori $\mathring{T}_{(\theta,\psi)} \subseteq D^4_{(\theta,\psi)}$, we obtain the embedded 4–manifold

$$W' := \bigcup_{(\theta,\psi)\in\mathbb{T}^2} \mathring{T}_{(\theta,\psi)} \approx \mathbb{T}^2 \times (\text{the punctured torus}) \subseteq S^6.$$

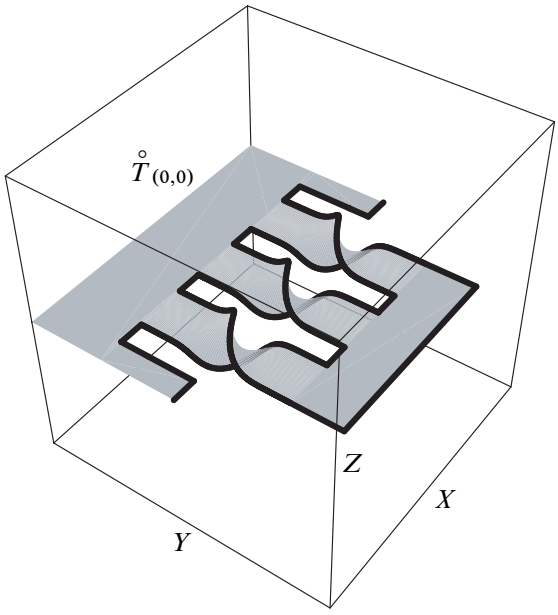

Figure 3: The Seifert surface for $\theta = \psi = 0$ in $\{w = 0\}$.

Then

$$W := \overline{\mathbb{B}^4 \smallsetminus \bigcup_{(\theta,\psi)\in\mathbb{T}^2} \mathbb{B}^2_{(\theta,\psi)}} \cup \bigcup_{(\theta,\psi)\in\mathbb{T}^2} \mathring{T}_{(\theta,\psi)} = \overline{\mathbb{B}^4 \smallsetminus \bigcup_{(\theta,\psi)\in\mathbb{T}^2} \mathbb{B}^2_{(\theta,\psi)}} \cup W'$$

becomes a smoothly embedded 4–manifold.

In each $D^4_{(\theta,\psi)}$ the thick arc (smoothed) gives our deformation $\bigcup_{\tau\in\mathbb{T}^2} \Phi(\tau)(D^1)$ and the rest of ∂W is $\overline{S^3 \smallsetminus (\mathbb{T}^2 \times D^1)}$. Therefore, W is a Seifert surface bounded by the knot $\Sigma^3_\Phi \subseteq S^6$. We abuse notation and identify $W \subseteq S^6$ with the image of an embedding $\widetilde{J}\colon W \hookrightarrow S^6$.

4.2 The second homology group

Now let us compute the second homology group $H_2(W;\mathbb{Z})$ of our Seifert surface W and its intersection form.

Since W' is diffeomorphic to $\mathbb{T}^2 \times$(the punctured 2–torus), we have

$$H_2(W') \approx \mathbb{Z} \oplus \mathbb{Z} \oplus \mathbb{Z} \oplus \mathbb{Z} \oplus \mathbb{Z},$$

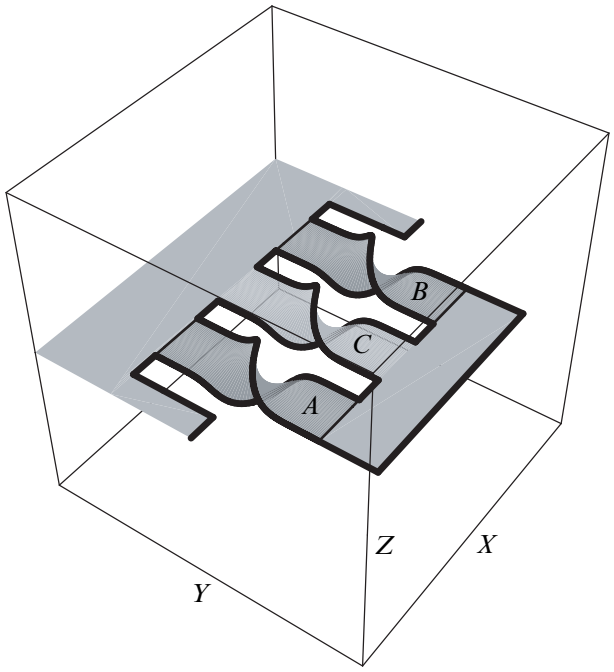

Figure 4: The bands A and B of $\mathring{T}_{(0,0)}$ are shown here in darkened gray, the disk C in light gray.

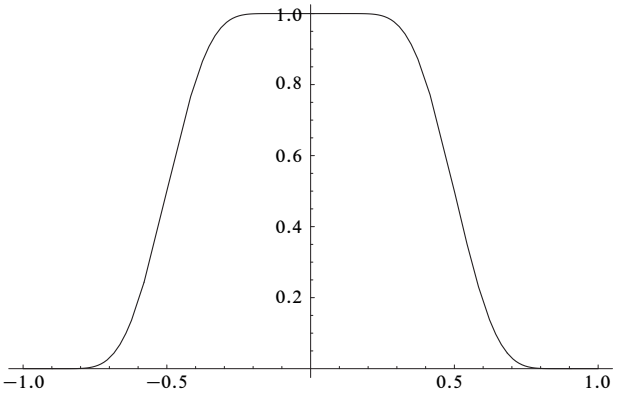

Figure 5: The bump function

by the Künneth lemma. If we take two closed curves α, β in the punctured torus $\mathring{T}_{(0,0)}$ at $(0,0) \in S^1_\theta \times S^1_\psi$ as shown in Figure 8, then the above five $\mathbb{Z}$s are generated

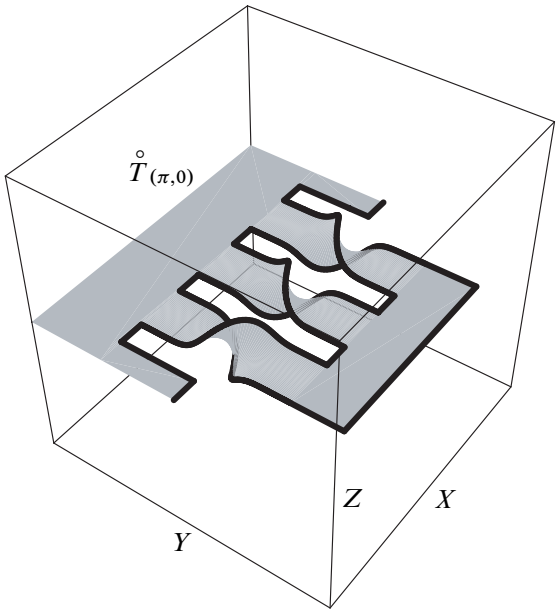

Figure 6: The Seifert surface for $\theta=\pi, \psi=0$ in $\{w=0\}$. Note the twist of the A band is reversed if compared to Figure 3.

by the five tori

$$T_{\alpha\theta}:=\alpha\times S^1_\theta,\quad T_{\alpha\psi}:=\alpha\times S^1_\psi,\quad T_{\beta\theta}:=\beta\times S^1_\theta,\quad T_{\beta\psi}:=\beta\times S^1_\psi \quad \text{and } \{*\}\times S^1_\theta\times S^1_\psi,$$

each embedded in W'. Here $*$ is a point of $\mathring{T}_{(0,0)}$.

Since W is obtained by gluing $\overline{D^4\smallsetminus \mathbb{T}^2\times D^2}$ ($\approx$ the 4–disk) to W' along a part of their boundaries, killing $[\{*\}\times S^1_\theta\times S^1_\psi]\in H_2(W')$, we have

$$\begin{aligned} H_2(W) &\approx \mathbb{Z}\oplus\mathbb{Z}\oplus\mathbb{Z}\oplus\mathbb{Z} \\ &\approx \langle[T_{\alpha\theta}]\rangle\oplus\langle[T_{\beta\psi}]\rangle\oplus\langle[T_{\alpha\psi}]\rangle\oplus\langle[T_{\beta\theta}]\rangle, \end{aligned}$$

by the Mayer–Vietoris sequence.

Among the above representatives of $H_2(W)$, the two pairs of "complementary" tori have intersection number 1. That is, the only non-zero intersection numbers are

$$[T_{\alpha\theta}]\cdot[T_{\beta\psi}]=[T_{\alpha\psi}]\cdot[T_{\beta\theta}]=1,$$

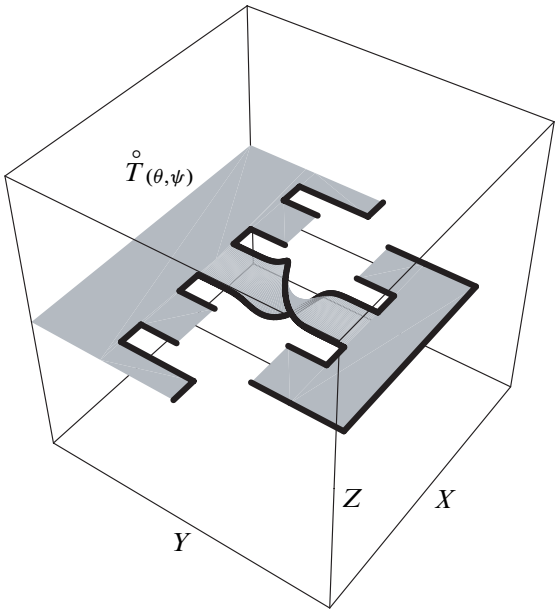

Figure 7: Generically, for $\theta, \psi \neq 0,$ or π the only parts of the two bands that appear in $\{w = 0\}$ are the center lines.

where $\cdot$ denotes the intersection pairing. Hence, with respect to the above generators, the intersection form on $H_2(W)$ is expressed as

$$\begin{pmatrix} 0&1&0&0\\ 1&0&0&0\\ 0&0&0&1\\ 0&0&1&0 \end{pmatrix}.$$

Note that the signature $\sigma(W) = 0$.

4.3 The normal Euler class

We compute the normal Euler class $e_{\widetilde{J}}$ for the embedding $W \hookrightarrow S^6$ using an intersection argument.

First note that any embedding of an oriented 3–manifold in S^6 has trivial normal bundle since it is unique up to regular homotopy and hence is regularly homotopic to an embedding in S^5. Take a small generic perturbation $\widehat{W}$ of W in S^6 and put $F := \widehat{W} \cap W$. Since $\Sigma^3_\Phi = \partial W \subseteq S^6$ has trivial normal bundle, $F \subseteq \operatorname{Int} W$ and the homology class $[F] \in H_2(W) \approx H_2(W, \partial W)$ is dual to the normal Euler class $e_{\widetilde{J}}$.

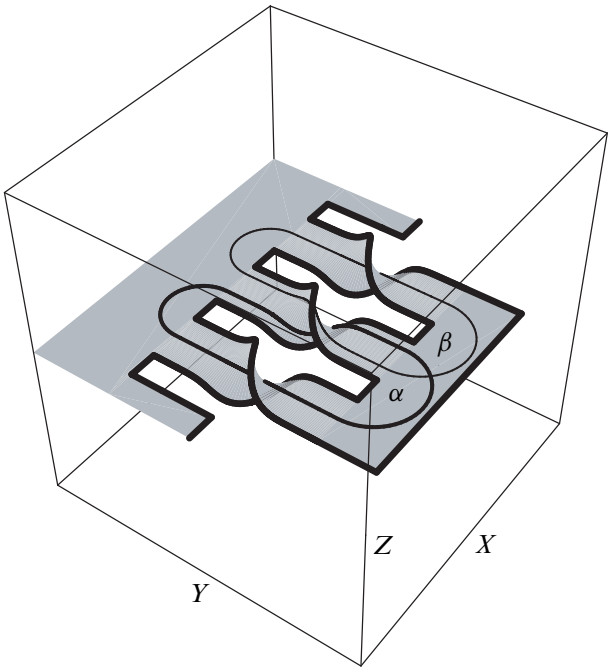

Figure 8: The loops α and β

With respect to the generators of $H_2(W)$ given in Section 4.2, we represent the class $[F]$ as

$$\begin{aligned}[F] &= a_1[T_{\alpha\theta}] + a_2[T_{\beta\psi}] + a_3[T_{\alpha\psi}] + a_4[T_{\beta\theta}] \\ &= (a_1, a_2, a_3, a_4) \in H_2(W) \cong \mathbb{Z} \oplus \mathbb{Z} \oplus \mathbb{Z} \oplus \mathbb{Z}.\end{aligned}$$

Then, with the intersection form in Section 4.2, we have, for example

$$a_2 = [F] \cdot [T_{\alpha\theta}].$$

If we let $\widehat{T}_{\alpha\theta} \subseteq \widehat{W}$ be the perturbation of $T_{\alpha\theta}$, then $a_2 = [F] \cdot [T_{\alpha\theta}]$ is equal to the intersection F and $\widehat{T}_{\alpha\theta}$ in $\widehat{W}$. This is further equal to the intersection of W and $\widehat{T}_{\alpha\theta}$, since $F = \widehat{W} \cap W$. Since $\widehat{T}_{\alpha\theta}$ can be thought of as a push-off of $T_{\alpha\theta} \subseteq W$ into $S^6 \smallsetminus W$, we only need to count the intersection of W and a push-off of $T_{\alpha\theta}$. By the same method, we can compute a_1, a_3, a_4 and hence the class $[F]$ dual to the normal Euler class $e_{\widetilde{\mathcal{J}}}$. We carry out this calculation below.

First, the punctured 2–torus $\overset{\circ}{T}_{(0,0)}$ at $(\theta, \psi) = (0, 0)$ lies in the 3–dimensional hyperplane $\{w = 0\}$, the hyperplane section by $w = 0$ of the normal 4–disk $D^4_{(0,0)}$. Consider

a vector field ν normal to the punctured 2–torus $\mathring{T}_{(0,0)}$ in this 3–dimensional hyperplane $\{(x, y, z, 0)\}$. In each normal 4–disk $D^4_{(\theta,0)}$, we consider $(\theta, 0) \times \alpha \subseteq \mathbb{T}^2 \times D^4$ to be sitting in $\mathring{T}_{(\theta,0)}$ and push it off along the same normal vector field ν. This determines a push-off $\widehat{T}_{\alpha\theta}$ of the 2–torus $T_{\alpha\theta}$ in S^6.

In each normal 4–disk $D^4_{(\theta,0)}$, $W \cap D^4_{(\theta,0)} = \mathring{T}_{(\theta,0)}$. As we vary θ, this punctured torus, outside the A–band, lies in the 3–dimensional hyperplane $\{w = 0\}$ and the A–band lies in $\{(x, y, t\cos\theta, t\sin\theta) | t \in \mathbb{R}\}$. Therefore, the only way that W and $\widehat{T}_{\alpha\theta}$ could intersect is when $(\theta, \psi) = (\pi, 0)$.

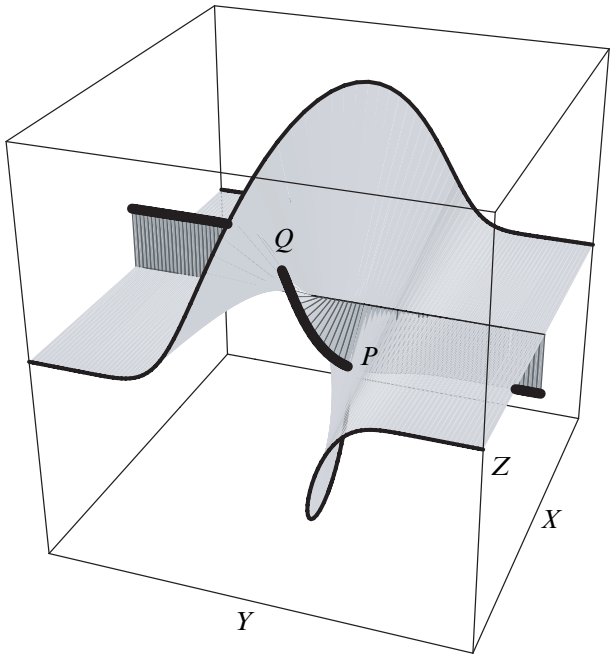

Figure 9: Intersection of $\widehat{T}_{\alpha\theta}$ and W. We see the A–band of $\mathring{T}_{(\pi,0)} \subseteq W$. A part of $T_{\alpha\theta}$ is shown as a straight thin line segment parallel to the y–axis. The push-off $\widehat{T}_{\alpha\theta}$ is a bold curve. For visualization, we show the trace of this push-off.

When $(\theta, \psi) = (\pi, 0)$, in the normal 4–plane $D^4_{(\pi,0)}$, the whole A–band lies in the 3–dimensional hyperplane $\{w = 0\}$. Figure 9 depicts the situation near the A–band in this 3–dimensional plane, where $\widehat{T}_{\alpha\theta}$ is viewed as a "half-twisted arc" and the B–band is an oppositely half-twisted band (Compare Figures 3 and 6). We see that the intersection of W and $\widehat{T}_{\alpha\theta}$ consists of the two points P and Q, seen in Figure 9.

However, it is not easy to see from Figure 9 the crucial fact that these intersections actually have the same sign. For this we use Figure 10.

Figure 10 shows a 3–dimensional sub-disk of W intersecting a 2–dimensional sub-disk of $\widehat{T}_{\alpha\theta}$ transversely in 5–dimensional space. The array of black dots represent a square patch S of $\widehat{T}_{\alpha\theta}$. The arrow in each figure represents a line segment of an A–band in W; thus the array of these segments represents a 3–cube of W.

This placement of the arrow depends on two sorts of twists — a half twist in the band in the y–direction and a full twist in the θ direction. To help visualize this, we use disks in gray. The half twist takes place within this disk while (simultaneously) the full twist has the effect of rotating this disk about the x–axis. These disks in gray are not part of our construction but only serve to guide visualization of the 3–dimensional graphics. For example, note that in the right side of the second row we do not see the dot. This is because as we go along this row, the dot is rotating in the xz–plane, and the disk has been rotated along the x–axis. The points of the disk with negative z–coordinate have positive w–coordinate so that our dot is hidden from view by this disk.

Not shown is a sixth coordinate — the ψ direction. This is a fourth coordinate for W and the sixth coordinate of the ambient space — this coordinate will not be considered for analysis here. What really matters is the normal bundle to W and tangent plane to the torus and these can be clearly understood using this figure. The θ corresponds to twisting of the first band A and is independent from the twisting with respect to ψ.

In the fifth row of Figure 10 the arrow and the dot for each value of y are both in the xz–plane in $\{w = 0\}$. The one-parameter family of these two-dimensional figures, when stacked, give rise to the three dimensional Figure 9.

We will be concerned with the two intersection points of our torus $\widehat{T}_{\alpha\theta}$ and the 4–manifold W. In Figure 10 these points occur where the black dot lies exactly on the arrow — P in row 5 column 3; and Q in row 5 column 7. Choose an orientation of the tangent bundle of $\widehat{T}_{\alpha\theta}$ and an orientation of the normal bundle of W. Transversality assures that, at each point of $W \cap \widehat{T}_{\alpha\theta}$, we can identify two-dimensional fibers of these bundles. The sign at the intersection point P is $+1$ if the two orientations agree, and -1 if not.

The square patch S of $\widehat{T}_{\alpha\theta}$ is flat in the θxyz–cube, thus its tangent plane coincides with this square S. Specifically, orient $\widehat{T}_{\alpha\theta}$ with vectors τ_y in the y direction (that is along the rows from left to right in Figure 10) and τ_θ the θ direction (down the columns of Figure 10). This ordered pair (τ_y, τ_θ) gives an orientation of the tangent plane of $\widehat{T}_{\alpha\theta}$. Next we choose a framing for the normal bundle for W. The normal

2–disks to W are all represented as disks normal to the arrow. In row 5 column 1 we orient the normal disk W by a vector pair (ω_1, ω_2) where ω_1 is in the direction of the z–axis and ω_2 in direction of the w–axis. Continuing in the fifth row, we choose ω_1 orthogonal to the arrow in the gray disk and ω_2 in the direction of the w–axis. (The details of the normal frames in other rows will not need to be considered in our analysis.)

We first focus on τ_y at P — row 5 column 3. As we go from left to right, the arrow rotates in the xz–plane while the dot rotates in the opposite direction where we view y as "time". At P, τ_y corresponds to the velocity vector of the dot with y viewed as time. At P the dot goes from the positive side of the arrow (with respect to ω_1) orthogonally to the negative side. Therefore τ_y has direction $-\omega_1$ at P. Similarly at Q (row 5 column 3) the dot goes from the negative side back to the positive side. Thus at Q, τ_y has direction $+\omega_1$. This can be seen also in Figure 9.

Next we consider τ_θ at P. This second tangent direction is downwards the third column. Note that as the dot passes P it goes from below the disk (that is, hidden from view) to above it (visible). This is in the direction of the positive w–axis. Thus at P, τ_θ is in the direction ω_2. At Q we see the dot go from above the disk to below it and so at Q, τ_θ is in the direction $-\omega_2$. This information is not apparent in Figure 9.

In summary the intersection numbers at P and Q are both -1. However, this sign depends on our choice of orientation of $\widehat{T}_{\alpha\theta}$, so we can only conclude that the signs at P and Q are the same.

Thus, we conclude

$$a_2 = [F]\cdot[T_{\alpha\theta}] = \pm 2.$$

By the same argument for β, ψ and the B–band instead of α, θ and the A–band, we have $a_1 = \pm 2$.

For the two tori $[T_{\alpha\psi}]$ and $[T_{\beta\theta}]$, we can easily check that their push-offs along the same normal field ν do not intersect W at all. Therefore, we have $a_3 = a_4 = 0$.

Finally, the homology class dual to the desired normal Euler class is

$$[F] = (\pm 2, \pm 2, 0, 0) \in H_2(W) \cong \mathbb{Z}\oplus\mathbb{Z}\oplus\mathbb{Z}\oplus\mathbb{Z}.$$

Thus, we have:

Proposition 4.1 $e_{\widetilde{J}} = (\pm 2, \pm 2, 0, 0) \in H^2(W)$.

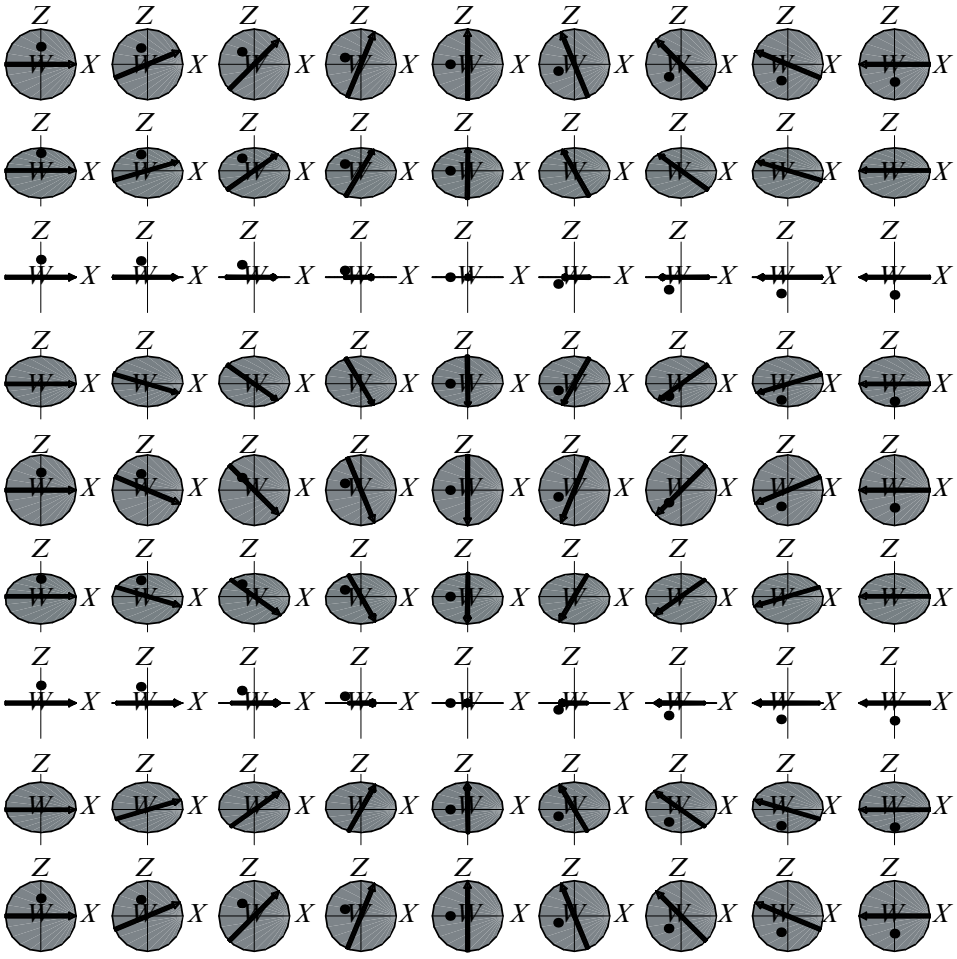

Figure 10: Local pictures of $\hat{T}_{\alpha\theta}$ (dots) and W (arrows). The horizontal rows correspond to the y–direction and the vertical columns correspond to the θ–direction.

4.4 Proof of Theorem 3.1

To prove Theorem 3.1, we have only to compute the Haefliger invariant $\mathsf{H}(J)$ for our spun knot $\Sigma^3_\Phi \subseteq S^6$ by using its Seifert surface $W \subseteq S^6$ constructed in Section 4.1.

By Theorem 2.1, together with Proposition 4.1, we have

$$\mathsf{H}(J) = -(\sigma(W) - e_{\tilde{J}} \smile e_{\tilde{J}})/8 = \pm(2\times 2 + 2\times 2)/8 = \pm 1.$$

This completes the proof of Theorem 3.1. □

5 Remarks

In view of the proof in Section 4.4, we easily see the following.

Remark 5.1 In the construction of $\Sigma^3_\Phi \subseteq S^6$, by using $\Phi'(\theta,\psi) := \Phi(m\theta, n\psi)$ $(m,n \in \mathbb{Z})$ for spinning (i.e. if we change the speed of the resolutions), we obtain the spun knot representing mn times the generator represented by Σ^3_Φ in C^3_3.

All of our arguments are valid for higher-dimensional Haefliger knots C^{2k+1}_{4k-1}, $k \geq 2$. First of all, Budney's resolution map is actually defined also in higher dimensions [4, Section 3] and our construction of the spun knot works there. Furthermore, since we also have higher-dimensional versions of Theorem 2.1 (see [19, Theorem 2.3] and [18, Theorem 5.1]), the proof is directly extended in high dimensions. Namely, we have:

Remark 5.2 If we deform-spin $S^{4k-1} \subseteq S^{6k}$ about

$$S^{2k-1} \times S^{2k-1} \subseteq S^{4k-1} \subseteq S^{6k}$$

via the higher-dimensional Budney map [4, Section 3]

$$S^{2k-1} \times S^{2k-1} \to \mathcal{K}_{2k+2,1}$$

(which corresponds to the case where we put $n = 2k+2$ in Budney's description of the generator of $\pi_{2n-6}\mathcal{K}_{n,1}$ [4, Section 3]), then the resultant spun knot represents a generator of C^{2k+1}_{4k-1} for $k \geq 1$.

All the steps of the proof parallel those of the case $k = 1$ (Section 4) with little alteration. In constructing the resolution map and the Seifert surface, we need to consider smooth proper arcs inside the normal $(2k+2)$–disk at each point of $S^{2k-1} \times S^{2k-1} \subseteq S^{6k}$, where we consider $S^{2k-1} \times S^{2k-1}$ to be the boundary of a tubular neighborhood of an unknotted S^{2k-1} in $S^{4k-1} \subseteq S^{6k}$.

References

[1] **E Artin**, *Zur Isotopie zweidimensionaler Flächen im* $\mathbb{R}^4$, Abh. Math. Sem. Univ. Hamburg 4 (1925) 174–177

[2] **J Boéchat**, *Plongements de variétés différentiables orientées de dimension* $4k$ *dans* $\mathbb{R}^{6k+1}$, Comment. Math. Helv. 46 (1971) 141–161 MR0295373

[3] **J Boéchat**, **A Haefliger**, *Plongements différentiables des variétés orientées de dimension* 4 *dans* $\mathbb{R}^7$, from: "Essays on Topology and Related Topics (Mémoires dédiés à Georges de Rham)", Springer, New York (1970) 156–166 MR0270384

[4] **R Budney**, *A family of embedding spaces*, Max Planck Institute for Mathematics Preprint Series MPIM2007-34 `arXiv:math.AT/0605069`

[5] **R Budney**, **J Conant**, **K P Scannell**, **D Sinha**, *New perspectives on self-linking*, Adv. Math. 191 (2005) 78–113 MR2102844

[6] **S Cappell**, *Superspinning and knot complements*, from: "Topology of Manifolds (Proc. Inst., Univ. of Georgia, Athens, Ga., 1969)", Markham, Chicago, Ill. (1970) 358–383 MR0276972

[7] **R H Fox**, *Rolling*, Bull. Amer. Math. Soc. 72 (1966) 162–164 MR0184221

[8] **G Friedman**, *Knot spinning*, from: "Handbook of knot theory", Elsevier B. V., Amsterdam (2005) 187–208 MR2179262

[9] **T G Goodwillie**, *A multiple disjunction lemma for smooth concordance embeddings*, Mem. Amer. Math. Soc. 86 (1990) MR1015675

[10] **L Guillou**, **A Marin**, *Commentaires sur les quatre articles précédents de V. A. Rohlin*, from: "À la recherche de la topologie perdue", Progr. Math. 62, Birkhäuser, Boston (1986) 25–95 MR900246

[11] **A Haefliger**, *Knotted* $(4k-1)$*–spheres in* $6k$*–space*, Ann. of Math. (2) 75 (1962) 452–466 MR0145539

[12] **A Haefliger**, *Differential embeddings of* S^n *in* S^{n+q} *for* $q > 2$, Ann. of Math. (2) 83 (1966) 402–436 MR0202151

[13] **W-C Hsiang**, **B J Sanderson**, *Twist-spinning spheres in spheres*, Illinois J. Math. 9 (1965) 651–659 MR0189047

[14] **R A Litherland**, *Deforming twist-spun knots*, Trans. Amer. Math. Soc. 250 (1979) 311–331 MR530058

[15] **R J Milgram**, *On the Haefliger knot groups*, Bull. Amer. Math. Soc. 78 (1972) 861–865 MR0315728

[16] **D Roseman**, *Spinning knots about submanifolds; spinning knots about projections of knots*, Topology Appl. 31 (1989) 225–241 MR997490

[17] **A Skopenkov**, *Classification of smooth embeddings of* 3*–manifolds in the* 6*–space* `arXiv:math.GT/0603429`

[18] **M Takase**, *A geometric formula for Haefliger knots*, Topology 43 (2004) 1425–1447 MR2081431

[19] **M Takase**, *The Hopf invariant of a Haefliger knot*, Math. Z. 256 (2007) 35–44

[20] **E C Zeeman**, *Unknotting spheres*, Ann. of Math. (2) 72 (1960) 350–361 MR0117738

[21] **E C Zeeman**, *Twisting spun knots*, Trans. Amer. Math. Soc. 115 (1965) 471–495 MR0195085

Department of Mathematics, University of Iowa
14 MacLean Hall, Iowa City IA 52242-1419, USA

Department of Mathematical Sciences, Faculty of Science, Shinshu University
Matsumoto, Nagano 390-8621, Japan

roseman@math.uiowa.edu, takase@math.shinshu-u.ac.jp

http://www.math.uiowa.edu/~roseman/

Received: 10 October 2006